NBSIR 84-3015

A PRELIMINARY INVESTIGATION INTO USING THE SUN AS A SOURCE FOR G/T MEASUREMENTS

NBSIR 84-3015

A PRELIMINARY INVESTIGATION INTO USING THE SUN AS A SOURCE FOR G/T MEASUREMENTS

William C. Daywitt

Electromagnetic Fields Division
National Engineering Laboratory
National Bureau of Standards
U.S. Department of Commerce
Boulder, Colorado 80303

August 1984

CONTENTS

A Preliminary Investigation Into Using the Sun as a Source for G/T Measurements

William C. Daywitt

Electromagnetic Fields Division
National Bureau of Standards
Boulder, Colorado 80303

This report describes a preliminary investigation into determining the solar flux density, the atmospheric correction factor, and the star shape correction factor for use in G/T measurements above 5 GHz. An estimate of errors is also included. Preliminary results show: an improved algorithm for determining diffusive and refractive attenuation; a viable technique for estimating the solar flux density from daily AFGL flux density measurements and a centimeter/millimeter wave spectrum function; and the possibility of reducing star shape correction factor errors by use of an effective solar rf diameter.

Key words: atmospheric correction factor; earth terminal measurement system; error analysis; G/T; solar flux density; star shape correction factor.

1. Background and Introduction

The Electromagnetic Fields Division of the National Bureau of Standards has successfully made precision G/T (gain to system noise temperature) measurements [1] on low noise, large diameter (11 m to 28 m) antenna systems using the radio star Cassiopeia A, and on medium size (4 m to 6 m) antenna systems using the moon. Although the moon is an attractive source to use with these smaller systems because of its predictable radio output [2], in many cases [3] the system noise is so much greater than the received lunar output that the measurement sensitivity is too low to be useful. Since the solar angular diameter is about that of the moon and its output is considerably greater, the sun provides an answer to the sensitivity problem. Unfortunately, its flux density and brightness distribution are variable, and even with this preliminary study a number of investigations are still needed to determine the correct G/T measurement error. This report describes an effort to determine the feasibility of using the daily Air Force Geophysics Laboratory (AFGL) flux density values [4] measured at the Air Force Sagamore Hill Observatory in Hamilton, Massachusetts. The results pertain to frequencies above 5 GHz for reasons that will be made clear later.

The antenna system G/T can be expressed as

$$\frac{G}{T} = \frac{8\pi k(Y-1)}{\lambda^2 S k_1 k_2} \tag{1}$$

where k is Boltzmann's constant, Y is the ratio of the power measured with the sun in the antenna mainbeam to the power measured with the antenna pointed at the cold sky, λ is the measurement wavelength, S is the solar flux density incident on the earth's atmosphere, and k_1 and k_2 are the atmospheric transmission and star shape correction factors respectively [5].

1

The atmospheric transmission factor accounts for the reduction in the received flux and is due to three atmospheric phenomena [6], gaseous attenuation, refractive spreading of the incident wavefront, and incoherent tropospheric scattering. It does not include attenuation and scattering from clouds, rain, fog, hail, or snow since the precision measurements envisioned here are assumed to be performed in clear, stable weather. If A is the total zenith attenuation in decibels due to these three phenomena, then

$$k_1 = 10^{-A/10\sin\theta} \tag{2}$$

where θ is the elevation angle to the source relative to the antenna location on the earth's surface. Details of a simplified calculation for the gaseous component of A are described elsewhere [7].

An algorithm derived in an earlier analysis [5] for the zenith attenuation due to the tropospheric scatter of the energy from a point source radio star and intended for the 1 GHz to 10 GHz frequency range diverges above 10 GHz. Since that analysis, further measurement data [8] has come to light which provides a more detailed picture of this attenuation. The resulting curves derived from the data and which include the refractive attenuation are shown in figure 1. The first set of data [6] were taken at 4.17 GHz and 6.39 GHz with a 22 m antenna, and the second set [8] at 15.5 GHz and 31.6 GHz with a 7 m antenna. The dashed curves through the two sets of data points are parallel, and suggest a family of straight lines for other antenna diameters. A linear interpolation in antenna diameter between the two dashed curves produced the linear portions of the curves shown. Since theory [6] indicates that the attenuation decreases with decreasing frequency, the curves were extended accordingly. When the angular diameter of the source is finite, the attenuation is reduced [6], decreasing as the ratio of source diameter to antenna beamwidth increases. The equation in figure 1 descibes this effect [5] where d is the source diameter, θ_H is the half-power beamwidth, A_o is the zenith attenuation for a point source given by the curves in the figure, and A is the corresponding attenuation for the finite source diameter. An earlier investigation [5] indicates that the total error in these attenuation curves and the non-point source correction is probably in the neighborhood of 50%.

The star shape correction factor accounts for variation of the solar brightness distribution across the antenna beam pattern, and vanishes as the ratio of the angular source diameter to the antenna half-power beamwidth vanishes. In terms of a distribution B and a normalized power pattern P_n,

$$k_2 = \frac{\int B(\Omega)P_n(\Omega)\,d\Omega}{\int B(\Omega)\,d\Omega} \tag{3}$$

where Ω represents the two antenna pointing angles and $d\Omega$ is the differential solid angle. The integral in the denominator is equivalent to the flux density S.

Sections 2 and 3 present the results of a preliminary investigation into the determination of the flux density S and the star shape correction factor k_2.

2. Determination of the Solar Flux Density Above 5 GHz

2.1 Strategy

Solar radio emission is the result of three superimposed sources of radiation [9], the quiet, slow, and burst components. The quiet sun emission comes from unlocalized, thermal sources in the solar atmosphere (chromosphere and corona), and is constant over periods of months to years. The slow component also has a thermal origin and originates in local sources in the vicinity of sunspots and chromospheric plagues. These partially polarized sources have periods of days, weeks, or months. The burst components are the results of thermal, synchrotron, and plasma radiation from transient sources such as flares, and are partially polarized. Their recurrence frequency and period are small for the quiescent portion of the solar cycle, increasing to two or more per a 10-hour viewing day during the active portion, which suggests the possibility of making G/T measurements using the sun without encountering a burst during the process. The fact that the quiet and slow components have periods of greater than a day further suggests the possibility of using an average of two successive daily AFGL flux density values to determine the flux at the time of the G/T measurement taking place between the two AFGL measurements.

Figure 2 depicts the average solar flux density spectrum incident on the earth's atmosphere [10] with an insert [11] indicating the duration of the burst spectrum from 10 MHz to 30 GHz. The quiet component of the solar emission dominates above 5 GHz, at which frequency most of the burst components have disappeared and the slow component is falling off. The insert shows that the duration of the remaining burst continuum is short. Thus, the solar emission above 5 GHz is relatively stable from day to day as long as the type IV bursts are avoided, again suggesting a G/T measurement scheme using AFGL flux density values.

Superimposed on the graph of figure 2 are three sets of hashmarks representing monthly averages of AFGL flux density measurements (with atmospheric attenuation removed) [4] from January 1979 to May 1982. The measurement values approach the average quiet sun value between the "sunspot (s.s) max" and the "s.s. min" curves as the frequency increases. Thus, above the highest AFGL measurement frequency (15.4 GHz), apparently the average of the quiet sun curves can be used to determine the flux density incident on the earth's atmosphere. Following is an approximate equation giving this average that was derived by least-square fitting the average data corresponding to the quiet sun curves in the figure and in table 1 (from reference [10]):

$$\log S = 1.20 + 1.10 \ (\log f) + 0.179 \ (\log f)^2. \tag{4}$$

The flux density S and the frequency f are the same units as the figure. The following equations can be used to extrapolate between the AFGL measurement frequencies [12]:

$$S = S_1^c \ S_2^{1-c} \tag{5}$$

where

$$c \equiv \frac{\ln(f/f_1)}{\ln(f_2/f_1)} . \tag{6}$$

S has the same units ($W/M^2/Hz$) as the graph, and f_1 and f_2 correspond to S_1 and S_2,

3

respectively. The subscripts denote the two AFGL values of flux density and frequency between which the flux density S at frequency f is desired.

The preceding discussion suggests the following strategy for determining the solar flux density above 5 GHz: 1) if the G/T measurement frequency is 4.995 GHz, 8.8 GHz, or 15.4 GHz, use an average of two adjacent daily AFGL flux values; 2) if the measurement frequency is between two AFGL frequencies, use the average determined in 1) for both AFGL frequencies and translate the result to the desired frequency via eqs (5) and (6); and 3) if the frequency is above 15.4 GHz, use eq (4) to determine the flux density. Since the reported AFGL flux density values are corrected for bursts, it is only then necessary to insure that the G/T measurement did not take place during a burst.

To illustrate, suppose a series 10 GHz G/T measurements were performed in Boulder, Colorado, at various times between 7 a.m. (1400 u.t. (universal time)) and 5 p.m. (2400 u.t. local standard time on October 17, 18, 19, 1983. The appropriate AFGL flux density values (in units of 10^{-22} W/m/Hz) that bracket 10 GHz on these days are isolated in the box of figure 3 for the month in question [4]. The "C" value from eq (6) for the frequencies indicated (8.8 GHz, 10 GHz, 15.4 GHz) turns out to be 0.7716 (with f_1 = 8.8, f = 10, and f_2 = 15.4). Using this value, the flux densities in the box, and eq (5), the 10 GHz flux density values at the AFGL measurement time (approximately 1630 u.t.) on the 17th, 18th, 19th, and the 20th are 334, 321, 330, and 326, respectively. Linear interpolation between any appropriate two of these values will then yield the correct flux value for a specific Boulder G/T measurement time. Figure 4 is a reproduction of another page from the "Solar-Geophysical Data" report that indicates the time and size (in flux density units) of any bursts that have taken place during the days in which the G/T measurements were being performed. The data in the boxes show the larger microwave bursts taking place during the G/T measurement times in question (1400 u.t. to 2400 u.t.), and thus any G/T measurements performed during these bursts should be discarded. The smaller bursts shown in the figure, although somewhat arbitrarily excluded, have a less significant effect on the G/T measurement.

2.2 Flux Density

For simplicity the preceding illustration ignores atmospheric attenuation and the true earth-sun distance at the time of the G/T measurements. A complete flux density determination between AFGL frequencies proceeds as follows: 1) calculate the flux densities S_1 and S_2 corresponding to the appropriate two AFGL frequencies for the G/T measurement time between the two AFGL daily measurements; 2) adjust S_1 and S_2 for the true earth-sun distance (the values reported in figure 3 are normalized to 1 astronomical unit); 3) remove the effects of atmospheric attenuation from S_1 and S_2 via eq (2); 4) use eqs (5) and (6) to obtain the flux density S incident on the earth's atmosphere at the G/T measurement frequency; and 5) apply eq (2) a second time at the measurement frequency to obtain the flux density at the location on the earth's surface where the G/T measurement is performed. Above 15.4 GHz eq (4) can be used to estimate the flux density incident on the atmosphere, after which step 5 is applied.

Prior to, but not afterward, January 1980, AFGL removed the effects of atmospheric attenuation from their measurements and reported flux density values incident on the atmosphere. Therefore, the flux density values reported in figure 3 contain the atmospheric attenuation.

To illustrate, suppose a G/T measurement is performed at an antenna site in Boulder on October 17, 1983, as the sun transits the local meridian (1848 u.t. [13]). The AFGL flux density values measured earlier on the 17th and on the following day during meridian transit (1630 u.t. [13]) at the Sagamore Hill Observatory are reported (fig. 3) as 282 and 268 at 8.8 GHz, and as 588 and 587 at 15.4 GHz. By a linear extrapolation in time between these daily measurements, flux density values at 1848 u.t. of 280.6 and 587.9 are obtained for 8.8 GHz and 15.4 GHz, respectively. The true earth-sun distance (in units of 1 astronomical unit) at 1848 u.t. on the 17th was 0.996 [13]. Thus, the true flux density values at the G/T measurement time are a factor of 1.008 (0.996^{-2}) larger than the values reported by AFGL, or 282.8 and 592.6 for 8.8 GHz and 15.4 GHz, respectively.

The average solar declination during the AFGL and G/T measurements was a negative 9.4 degrees [13]. Combined with the Sagamore Hill latitude of 40.6° north, this leads to a solar elevation angle at that site of 38.0°. The zenith values for the gaseous component of the atmospheric attenuation in October at the observatory are [7] 0.042 dB and 0.080 dB for 8.8 GHz and 15.4 GHz, respectively. The zenith values for the diffusive and refractive attenuation for the average solar diameter of 0.58° [13] during the measurements are (fig. 1) 0.012 dB at 8.8 GHz and 0.015 dB at 15.4 GHz. Combining these with the gaseous components gives a total zenith attenuation of 0.054 dB at 8.8 GHz and 0.095 dB at 15.4 GHz. These latter values with the 38.0° declination lead via eq (2) to atmospheric correction factors of 0.980 at 8.8 GHz and 0.965 at 15.4 GHz. Dividing the previous flux density values by these correction factors leads to 288.6 and 614.1 at 8.8 GHz and 15.4 GHz, respectively, for the flux densities incident on the atmosphere. Equations (5) and (6) can now be used to obtain an estimate of the 10 GHz flux density and results in a value 342.9. If the Boulder site is at 40° north latitude, the solar elevation angle there is 40.6°. Combining a gaseous attenuation of 0.029 dB [7] with a diffusive and refractive attenuation of 0.011 dB (fig. 1) yields a correction factor of 0.986 for a 40.6° elevation angle, resulting in a value of 338.1 for the flux density at the Boulder site.

2.3 Errors

The total error in determining the flux density from the AFGL measurements is the sum of four parts: the AFGL measurement error; the error in using eqs (5) and (6) to extrapolate between AFGL frequencies; the error in estimating the atmospheric transmission factor; and the error in estimating the flux density by the linear time interpolation between the daily AFGL measurements. This latter error for frequencies above the highest AFGL frequency (15.4 GHz) is at present taken as the maximum error (halfway) between the highest AFGL frequencies, 8.8 GHz and 15.4 GHz.

The AFGL error for measuring the flux density is 5% [12].

An error of 1% is assigned to the uncertainty in extrapolating between AFGL frequencies, and was determined by comparing the 8.8 GHz average value (average of the AFGL hashmarks in figure 2) with the 8.8 GHz value obtained via eqs (5) and (6) and the average AFGL values at 4.995 GHz and 15.4 GHz.

The total (gaseous + diffusive + refractive) zenith attenuations for Boulder at 10 GHz and Sagamore Hill at 8.8 GHz and 15.4 GHz are 0.040 dB, 0.054 dB, and 0.095 dB, respectively. All of these values are uncertain by 50% [5], leading to transmission coefficient errors of 0.7%, 1.0%,

and 1.8%, respectively. The overall transmission coefficient error is a weighted sum $(0.7+c\times1.0+(1-c)\times1.8)$ of these separate errors with a value of approximately 2% for the value of C determined in section 2.1.

Figure 5 is a plot of a number of hypothetical smoothed flux density curves between the AFGL values of $S(t_1)$ and $S(t_2)$ <u>measured</u> during meridian passage at time t_1 and time t_2 the following day ($t_2 \doteq t_1$ + 24 hours). The linear curve whose equation is shown in the figure was previously used to estimate the flux density at time t between the AFGL measurement times t_1 and t_2, where h is the relative forward interval between t_1 and t. S(t) is the flux density at t for the true (but unknown) curve, and σ_S is the estimated standard deviation of the possible values at t for the probability density curve shown. The forward relative interval h is defined in the figure. ΔS is defined to be the difference between the linear approximation and the unknown flux density S(t), and is therefore a random variable whose estimated standard deviation σ_Δ is a measure of the error in using the linear approximation. A simple analysis of the situation depicted in the figure shows that the two standard deviations are related by the equation

$$\sigma_\Delta^2 = 2\sigma_S^2[1 - h + h^2 + h(1-h)\rho_1 - (1-h)\rho_1^h - h\rho_1^{1-h}] \tag{7}$$

where ρ_1 is the estimated autocorrelation function [14] between measured flux density values 24 hours ($\doteq t_2 - t_1$) apart. ρ_1^h and ρ_1^{1-h} are, respectively, approximations to the autocorrelation functions between flux density values $t - t_1$ and $t_2 - t$ apart. The flux-density variations are assumed to be sufficiently stationary for eq (7) to give some indication of the time interpolation error.

Figure 6 shows a plot of the 8.8 GHz AFGL flux density values measured from January through June 1979. The change of levels at L1, L2, and L3, and the slopes at S1, S2, and S3 indicate that the variation is not stationary and should possibly be modeled [14] as an ARIMA (p,1,q) or an ARIMA (p,2,q) process to estimate the standard deviation of the residual day-to-day fluctuations of interest. However, for a preliminary (and more conservative) estimate of σ_S, the data shown was assumed to be stationary, resulting in a value of 24 for σ_S and a value of 0.9 for ρ_1. With these values eq (7) is approximated by

$$\sigma_\Delta \approx 11(h-h^2)^{1/2} . \tag{8}$$

This equation shows a maximum of 5.5 halfway between t_1 and t_2, and is assumed to hold for the entire range from 5 GHz to 15.4 GHz. For the illustration in section 2.2, h has the value of 0.096 ((18.8-16.5)/24), yielding an estimated standard deviation from eq (8) of 3.2 or 1% (3.2/337), or a 3σ error of approximately 3%.

Collecting the previous errors leads to a total error of 11% (3σ) in determining the solar flux density for the illustration presented in section 2.2. The error at lower elevation angles and/or higher frequencies will be greater, primarily because of increased gaseous attenuation.

3. Star Shape Correction Factor

For antenna half-power beamwidths (HPBW) greater than about five angular source diameters, examination of eq (9) shows that ratio in eq (3) can be replaced by unity with an error less than

1%. To use the celestial-source method of measuring G/T accurately below five source diameters, however, an estimate of the variation of the source brightness distribution across the antenna mainbeam indicated in the numerator of eq (3) must be made. For sources with stable and predictable distributions and Gaussian mainbeams, this can be accomplished by replacing the ratio in eq (3) by a simple formula depending only upon the ratio of HPBW to source diameter. Furthermore, if the source diameter is properly chosen, the formula will provide an accurate estimate of the correction factor for any HPBW/diameter ratio above unity [15,2]. As will be seen there is reason to expect that this technique will also work for the sun, even though the solar brightness distribution is continuously changing. Errors in the star shape correction factor have not yet been investigated.

For a source resembling a circular disk and a Gaussian mainbeam, eq (3) leads to

$$k_2 = \frac{1 - e^{-x^2}}{x^2} \tag{9}$$

where

$$x^2 \equiv \left(\frac{d}{\theta_H}\right)^2 \ln2 . \tag{10}$$

d is the effective rf angular diameter of the source, and θ_H is the antenna HPBW. The diameter is chosen to minimize the difference

$$\frac{1 - e^{-x^2}}{x^2} - \frac{\int B(\Omega) P_n(\Omega) d\Omega}{\int B(\Omega) d\Omega} \tag{11}$$

for θ_H/d greater than unity. The same expressions (eqs (9) and (10)) hold for an elliptical disk with d^2 replaced by the product of the major and minor source diameters. No significant reduction in the difference in eq (10) is achieved with this latter model, however, even though the solar brightness distribution shows a decided ellipticity (fig. 7, [9]).

Figure 2 shows that, except for the burst components which are assumed to be missing during the G/T measurement, the quiet sun emission plays an increasingly dominant role in the total emission above 5 GHz where the slow component begins to fall off. Furthermore, observations of the solar brightness distribution in the decimeter, centimeter, and millimeter wave frequency regions reveal that, although the effective brightness temperature varies with the solar cycle, the distributions remain relatively constant [9]. It is this constant part of the brightness distribution that will presumably be amenable to the technique of the previous paragraph, with fluctuations in the result coming from the more variable slow emission component. The degree of success will depend upon how minor these fluctuations turn out to be, but hopefully at least some accuracy in k_2 will be gained below five source diameters. This question can only be decided after a number of distributions at various frequencies and at various times during the solar cycle have been convolved with the antenna beam pattern. To date this has not been done.

Since the effective diameter or diameters for the solar distributions have not yet been determined, the question of what diameter d to use in eq (10) remains. A glance at figure 7 shows

that the polar profiles tend to average out as a constant up to the optical diameter, with the equatorial profile averages extending somewhat beyond. This situation implies that the effective rf diameter will extend beyond the optical diameter, which in turn will depend upon the results from convolving the brightness distributions with the Gaussian beam pattern. Based on a circular disk model of the quiet-sun atmosphere with a constant chromospheric temperature of 3×10^4 kelvins and a coronal temperature of 10^6 kelvins, Smerd [16] calculated a brightness temperature distribution and compared it to the apparent brightness temperature derived from the same model. The apparent temperature is defined as the temperature of a blackbody having the same diameter as the optical disk and radiating the same apparent flux density. The results are shown in figure 8 where the ratio of two particular brightness temperature contours to the apparent temperature are plotted. The upper curve is where the contour temperature falls to 1% of the apparent temperature and the lower curve is where it falls to 10%. As expected the ratios approach unity with increasing frequency as the origin of the radiation is increasingly confined to the chromosphere. The dashed line approximating the 10% curve and ending at 30.3 GHz will be used temporarily to define the effective diameter for eq (10). Thus,

$$d = d_o \begin{cases} 1.240-0.162 \log f, & 5 \leqslant f \leqslant 30.3 \\ 1 & , f \geqslant 30.3 \end{cases} \tag{12}$$

where d_o is the optical diameter obtained from the Astronomical Almanac [13] at the time of the G/T measurement. For the illustration in section 2.2, the Boulder antenna diameter is 4.3 m (fig. 1) yielding a 10 GHz HPBW of 0.49°. At the measurement time the optical solar diameter was 0.54° [13] which yields an rf diameter via eq (12) of 0.58°. Equations (9) and (10) then give a star shape correction factor of 0.64.

4. Discussion and Conclusions

The curves in figure 1 used for determining the diffusive and refractive attenuation for a point source, although quite rough and incomplete, offer an improvement over the previous algorithm [5] that diverges above 10 GHz.

The total error in estimating the solar flux density from 5 GHz to 15.4 GHz in clear, stable, weather is 11%, and is the sum of 5% for the AFGL measurements, 1% for extrapolating between two AFGL frequencies, 3% for estimating the flux density between the daily AFGL measurement times, 1.3% for removing the atmospheric attenuation from the AFLG measurements, and 0.7% for estimating the atmospheric attenuation at the G/T measurement frequency. Discarding the 0.7% error, the sum comes to about 8%, and represents the error in determining the flux density incident on the earth's atmosphere. Since the average of the AFGL hashmarks in figure 2 approaches the area between the "s.s. max" and "s.s. min" curves as the frequency increases, and since their spread and that between the curves decreases with frequency, it appears that an 8% error in using eq (4) to determine the solar spectrum above 15.4 GHz incident on the earth's atmosphere is reasonable for the spectrum shown in the figure.

The brightness distribution of the quiet sun above 5 GHz is relatively insensitive to the solar cycle. This, coupled with the fact that the quiet-sun component also dominates above this frequency, implies the possibility of finding an effective rf diameter (as a function of frequency) that minimizes the error in using the circular disk approximation to the star shape

correction factor in eq (3), improving G/T measurement accuracy for HPBW/source-diameter ratios between one and five.

Although the preceding conclusions appear to be reasonable, there still remains a considerable amount of work to be completed before final acceptance.

The majority of the work described in this report was carried out in 1979 and was part of a larger effort to design and construct an earth terminal measurement system capable of precision antenna system measurements. Therefore, much of the direction and inspiration for this work came from other individuals associated with the project, principally David Wait and John Wakefield.

6. References

[1]   Wait, D. F. Precision measurements of antenna system noise using radio stars. IEEE Trans. on I&M, Vol. IM-32, No. 1: 110-116; 1983 March.

[2]   Daywitt, W. C. An error analysis for the use of presently available lunar radio flux data in broadbeam antenna-system measurements. Nat. Bur. Stand. (U.S.) Tech. Note 1073; 1984 February.

[3]   Wait, D. F.; Daywitt, W. C. Preliminary examination of 20 GHz G/T measurements of earth terminals. Nat. Bur. Stand. (U.S.) Int. Rpt. 83-1686; 1983 March.

[4]   Solar-Geophysical Data; prompt reports. Ed. H. E. Coffey; No. 470, Part 1, 1983 November.

[5]   Daywitt, W. C. Error equations used in the NBS precision G/T measurement system. Nat. Bur. Stand. (U.S.) Int. Rpt. 76-842, 1976 September.

[6]   Yokoi, H.; Yamada, M.; Satoh, T. Atmospheric attenuation and scintillation of microwaves from outer space. Publ. Astr. Soc. Japan, Vol. 22, No. 4, 511-524; 1970.

[7]   Daywitt, W. C. Atmospheric propagation equations used in the NBS earth terminal measurement system. Nat. Bur. Stand. Int. Rpt. 78-883, 1978 April.

[8]   Yokoi, H.; Yamada, M. Measurements of earth-space propagation characteristics at 15.5 GHz and 31.6 GHz using celestial radio sources. Trans. IECE '74/2, Vol. 57-B, No. 2; 121-128; 1974 February.

[9]   Kundu, M. R. Solar Radio Astronomy. New York, N.Y.: Interscience Publishers; 1965.

[10]   Allen, C. W. Astrophysical Quantities. London: The Athlone Press/University of London; 1976.

[11]   Mangis, S. J.   Introduction to solar-terrestrial phenomena and the space environment services center. NOAA Tech. Rpt. ERL 315-SEL 32, 1975 January.

[12]   Guidice, D. A.; Castelli, J. P.   The use of extraterrestrial radio sources in the measurement of antenna parameters.   IEEE Trans. Aerospace and Electronic Systems: Vol. AES-7, No. 2; 226-234; 1971 March.

[13]   The Astronomical Almanac for the Year 1983. Washington: U.S. Government Printing Office.

[14]   Box, G. E. P.; Jenkins, G. M.   Time Series Analysis--Forecasting and Control.   San Francisco: Holden-Day; 1976.

[15]   Kanda, M. An error analysis for absolute flux density measurements of Cassiopeia A.   IEEE Trans. on I&M, Vol. IM-25, No. 3; 173-182; 1976 September.

[16]   Smerd, S. F.   Radio-frequency radiation from the quiet Sun. Aus. J. Sci. Res., A3, 34; 34-59; 1950.
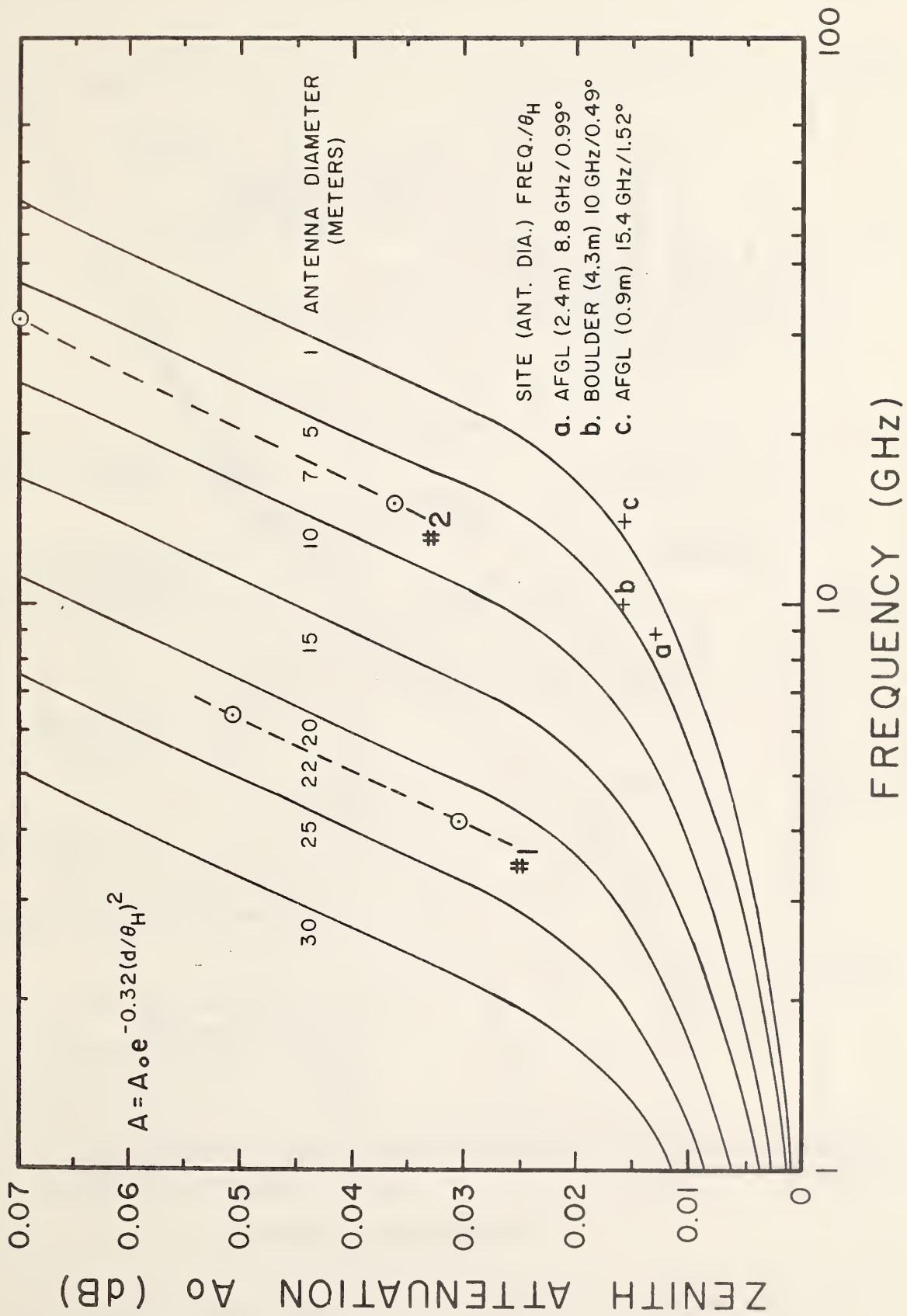
Figure 1. Diffusive and refractive attenuation A_0 for a point source. The equation appearing in the upper left corner of the figure is used to estimate the attenuation A for a non-point source ($d \neq 0$) once A_0 has been determined from the curves.

11
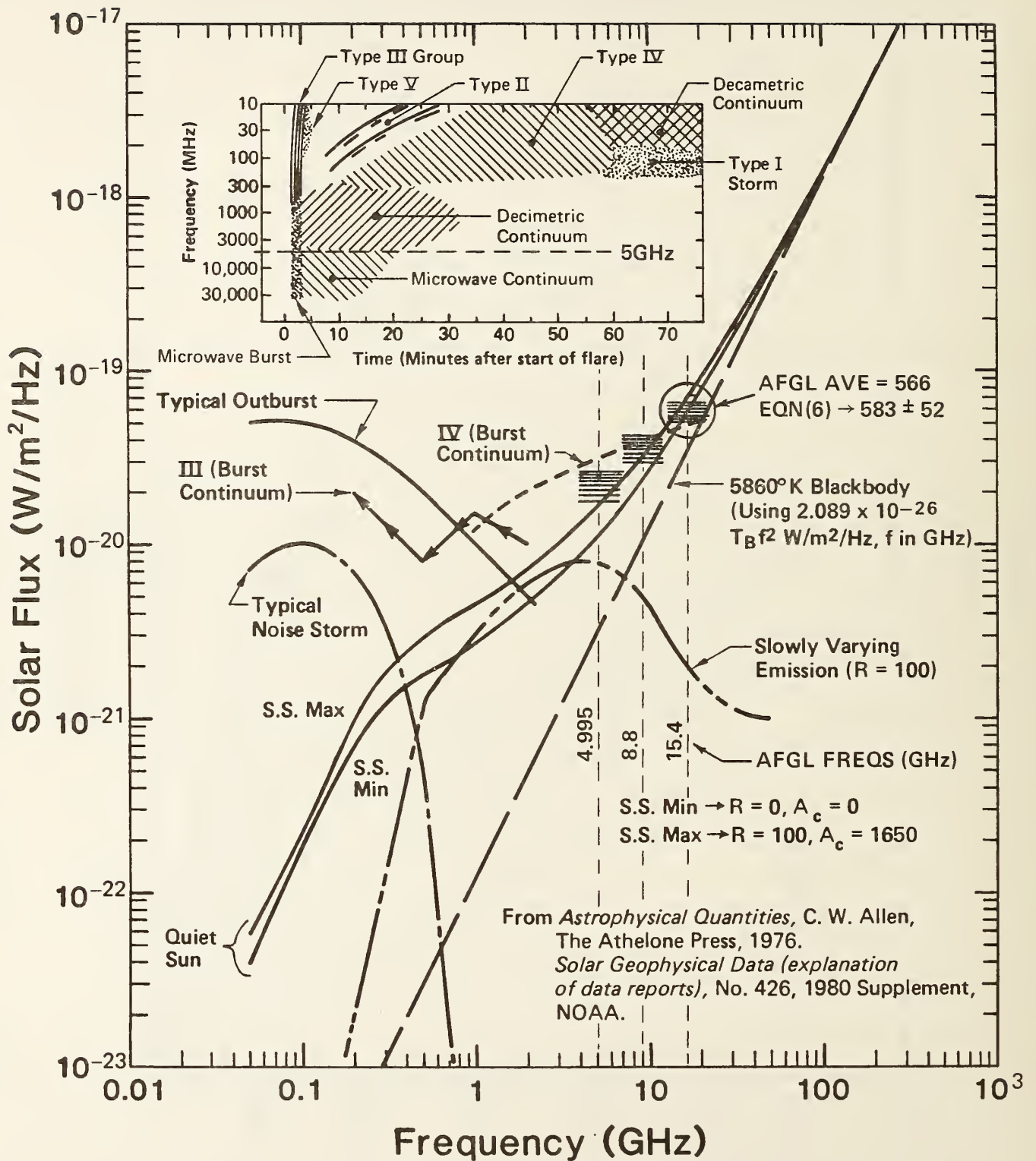
Figure 2. Solar radio spectrum. (The symbols are explained more fully in reference [10].)

D A I L Y   S O L A R   I N D I C E S

OCTOBER 1983

Day	Julian Day	Bartels Cycle Day	Sunspot Numbers R_I	R_A	Obs Flux Ottawa (2800)	----- Solar Flux Adjusted to 1 Astronomical Unit -----								
						SGMR (15400)	SGMR (8800)	SGMR (4995)	Ottawa (2800)	SGMR (2695)	SGMR (1415)	SGMR (606)	SGMR (410)	SGMR (245)
01	275	11	32	33	117.3	565	266	148	117.5	105	97	79	37	22
02	276	12	51	57	120.3	566	266	152	120.4	106	97	75	34	19
03	277	13	63	69	123.0	---	---	---	123.1	---	---	--	--	--
04	278	14	74	73	125.1	585	271	156	125.1	110	99	76	33	15
05	279	15	65	59	126.6*	586	286	160	126.6*	121	103	80	33	23
06	280	16	75	76	132.8	592	277	161	132.7	127	106	82	34	17
07	281	17	87	86	134.0	596	281	158	133.9	103	109	87	36	19
08	282	18	99	89	131.4*	582	280	157	131.1*	113	111	87	36	22
09	283	19	106	100	130.8	580	276	156	130.4	109	112	85	39	36
10	284	20	108	113	134.0*	601	277	160	133.6*	115	119	84	35	24
11	285	21	130	134	138.9	593	271	164	138.3	121	118	83	37	19
12	286	22	122	114	134.2	570	265	157	133.7	110	113	73	32	16
13	287	23	100	94	134.2*	554	296	173	133.5*	121	114	87	37	15
14	288	24	75	73	132.2*	618	299	175	131.5*	119	110	82	35	16
15	289	25	72	64	127.8	---	---	---	127.0	---	---	--	--	--
16	290	26	61	55	118.0A	605	284	161	117.2A	101	99	75	32	16
17	291	27	60	53	111.7*	588	282	152	110.9*	97	95	76	35	20
18	292	1	63	57	104.4	587	268	138	103.6	89	86	68	31	17
19	293	2	46	36	106.0	591	278	142	105.2	93	89	73	33	15
20	294	3	26	24	100.0	589	274	132	99.1	83	87	72	31	15
21	295	4	18	18	90.1	589	265	125	89.3	79	84	69	30	15
22	296	5	22	25	88.1	580	256	121	87.2	79	77	71	30	13
23	297	6	22	16	88.7	565	257	123	87.8	75	79	70	31	18
24	298	7	20	19	89.6	536	246	121	88.6	73	79	72	30	14
25	299	8	18	17	90.3	566	254	122	89.2	81	84	70	28	13
26	300	9	22	13	90.2	579	262	126	89.1	80	79	73	30	14
27	301	10	12	13	90.1	575	265	126	88.9	83	80	--	31	14
28	302	11	11	12	91.6	578	256	124	90.4	84	79	74	34	15
29	303	12	16	0	92.0	571	259	124	90.7	78	76	68	29	14
30	304	13	15	8	93.9	565	252	124	92.6	82	80	50	26	14
31	305	14	19	15	97.0*	585	262	128	95.5*	86	83	73	28	15
Mean			55	52	112.4	581	270	143	111.7	97	95	76	32	17

*Adjusted for burst in progress at time of measurement.

The observed and the adjusted Ottawa fluxes tabulated above are the "Series C" daily values reported by the Algonquin Radio Observatory, Ottawa, Ontario, Canada. The letter "A" following an entry designates an interpolated flux. Numbers in parentheses in the column headings denote frequencies in MHz.

Equipment problems produced the gaps shown here in the Air Weather Service's Sagamore Hill (SGMR) observations.

The International and American sunspot numbers shown above are preliminary values.

Figure 3. Smoothed solar flux density (in units of $W/m^2/Hz$) measured daily by the AFGL Sagamore Hill observatory (SGMR) at approximately solar meridian passage each day and adjusted to one astronomical unit. The box contains the flux densities of interest.

S O L A R   R A D I O   E M I S S I O N
S E L E C T E D   F I X E D   F R E Q U E N C Y   E V E N T S

OCTOBER   1983

Day	Freq	Sta	Type		Start (UT)	Time of Maximum (UT)	Duration (Min)	Flux Density Peak (10 -22 W/m 2 Hz)	Mean	Int	Remarks
17	8800	LEAR	8	S	0552.1	0552.8	1.7	24.0			QL=6 ST=2 TYP=3
	2695	LEAR	8	S	0552.3	0552.8	.8	10.0			QL=6 ST=2 TYP=3
	8800	LEAR	8	S	0940.1	0940.1	.4	30.0			QL=6 ST=2 TYP=3
	2695	LEAR	8	S	0940.1	0940.1	.5	20.0			QL=6 ST=2 TYP=3
	3200	8ERN	4	S/F	1140.5U	1141.0U	4.00	155.0U			ONLY PAPER REC
	8800	ATHN	4	S/F	1207.8	1213.5	12.8	21.0			QL=6 ST=2 TYP=3
	8800	SGMR	8	S	1213.1	1214.6	1.5	20.0			QL=6 ST=3 TYP=3
	2800	OTTA	21	GRF	1520.0		190.0	2.4			
	2800	OTTA	1	S	1634.0	1634.2	5.0	6.0	1.2		
	2800	OTTA	1	S	1658.0	1658.4	2.0	1.8			
	2800	OTTA	1	S	1718.9	1719.0	1.0	1.8	.8		
	2800	OTTA	8	S	2029.0	2029.3	.5	7.0			
18	8800	LEAR	20	GRF	0143.5	0144.8	7.5	9.0			QL=6 ST=2 TYP=2
	8800	LEAR	8	S	0346.3	0347.0	2.0	10.0			QL=6 ST=2 TYP=3
	8800	LEAR	4	S/F	0350.3	0351.0	8.7	9.0			QL=6 ST=2 TYP=3
	8800	SGMR	47	GB	1924.6	1925.6	3.7	139.0			QL=6 ST=2 TYP=5
	8800	PALE	47	GB	1924.8	1925.6	2.0	119.0			QL=6 ST=2 TYP=5
	2800	OTTA	3	S	2105.0	2106.5	5.0	10.4	4.0		
	2695	PALE	8	S	2106.0	2106.8	1.1	17.0			QL=6 ST=2 TYP=3
	8800	PALE	8	S	2106.3	2106.3	.5	27.0			QL=6 ST=2 TYP=3
19	2800	OTTA	240	R	1426.0	1431.0	5.0	2.4	1.6		
	2800	OTTA	1	S	1444.0	1447.0	7.0	8.0	3.0		
	2800	OTTA	21	GRF	1444.0	1450.0	40.0	2.4	1.2		
	2695	SGMR	8	S	1446.1	1446.6	1.2	16.0			QL=6 ST=2 TYP=3
	8800	SGMR	8	S	1446.5	1446.6	.6	16.0			QL=6 ST=2 TYP=3
	2800	OTTA	21	GRF	1750.0	1905.0	320.0	6.4			
	2800	OTTA	28	PRE	1959.0	2000.0	4.0	3.8	1.9		
	8800	SGMR	47	GB	1959.1	2009.3	15.4	200.0			QL=4 ST=2 TYP=5
	8800	PALE	8	S	1959.6	1959.8	1.0	45.0			QL=6 ST=2 TYP=3
	2695	PENT	4	S/F	2003.0	2009.2	15.0	265.0	34.0		
	8800	PALE	47	GB	2004.0	2006.1	15.6	160.0			QL=6 ST=2 TYP=5
	2695	PALE	47	GB	2005.8	2006.1	11.0	21.0			QL=6 ST=2 TYP=5
	2695	SGMR	47	GB	2005.8	2009.3	9.7	150.0			QL=4 ST=2 TYP=5
	2800	OTTA	29	PBI	2018.0	2018.0	130.0	11.8	4.9		
24	2695	PALE	8	S	1840.1	1840.3	.4	29.0			QL=6 ST=2 TYP=3
29	2800	OTTA	2	S/F	1925.5	1930.8	7.5	6.8	2.6		
	2800	OTTA	29	PBI	1933.0	1933.0	10.0	1.8	.9		
31	2800	OTTA	23	GRF	1610.0	1820.0	300.00	12.8			
	2800	OTTA	4	S/F	1613.0	1616.1	6.0	30.0	13.0		
	2695	SGMR	4	S/F	1615.1	1616.1	3.0	28.0			QL=6 ST=2 TYP=3
	2800	OTTA	29	PBI	1619.0	1619.0	20.0	5.2	2.6		

Reports are received routinely from the following observatories:

ATHN = Atnens	HUAN = Huancayo	NAGO = Nagoya	POTS = Potsdam
8ERN = Berne	IRKU = Irkutsk	NOBE = Nobeyama	SAOP = Sao Paulo
BORO = Bordeaux	IZMI = IZMIRAN	ONDR = Ondrejov	SGMR = Sagamore Hill
CRIM = Crimea	KISV = Kislovodsk	OTTA = Ottawa	TORN = Torun
OWIN = Owingeloo	KRAK = Krakow	PALE = Palehua	TYKW = Toyokawa
GORK = Gorky	LEAR = Learmonth	PEKG = Peking	TRST = Trieste
HIRA = Hiraiso	MANI = Manila	PENT = Penticton	UPIC = Upice
			VORO = Voroshilov

Explanation of Type Code:

1 Simple 1	7 Minor +	24 Rise	30 Post Burst Increase A	43 Onset of Noise Storm
2 Simple 1F	8 Spike	25 Rise A	31 Post Burst Decrease	44 Noise Storm in Progress
3 Simple 2	20 Simple 3	26 Fall	33 Absorption	45 Complex
4 Simple 2F	21 Simple 3A	27 Rise and Fall	40 Fluctuation	46 Complex F
5 Simple	22 Simple 3F	28 Precursor	41 Group of Bursts	47 Great Burst
6 Minor	23 Simple 3AF	29 Post Burst Increase	42 Series of Bursts	48 Major

1A Simple 1A	4A Simple 2AF	24PF Post Rise F	27F Rise and Fall F	
3A Simple 2A	240 Rise only	16A Fall A	27AF Rise and Fall AF	
21A Simple 3A GRF	240F Rise only F	260 Fall Only	31A Post Burst Decrease A	
2A Simple 1AF	24P Post Rise	26F Fall F	32A Absorption A	
			46F Complex F	

Remarks:
QL = Quality (1=poor to 6=excellent)
ST = Status (1=real time; 2=final; 3=correction; 4=deletion)
TYP= Type (1=noise storm;2=rise in base level;3=minor;4=group;5=major;6=major plus;7=Castelli U-type burst)

Figure 4.   Selected, short duration, radio emissions.   Major events to be avoided during the G/T measurement days are contained in the boxes.
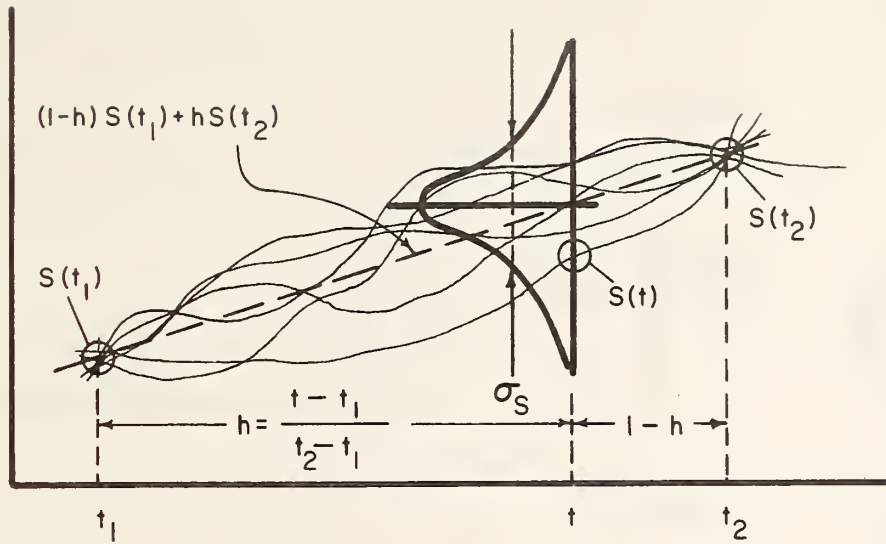
Figure 5. Hypothetical flux density curves.
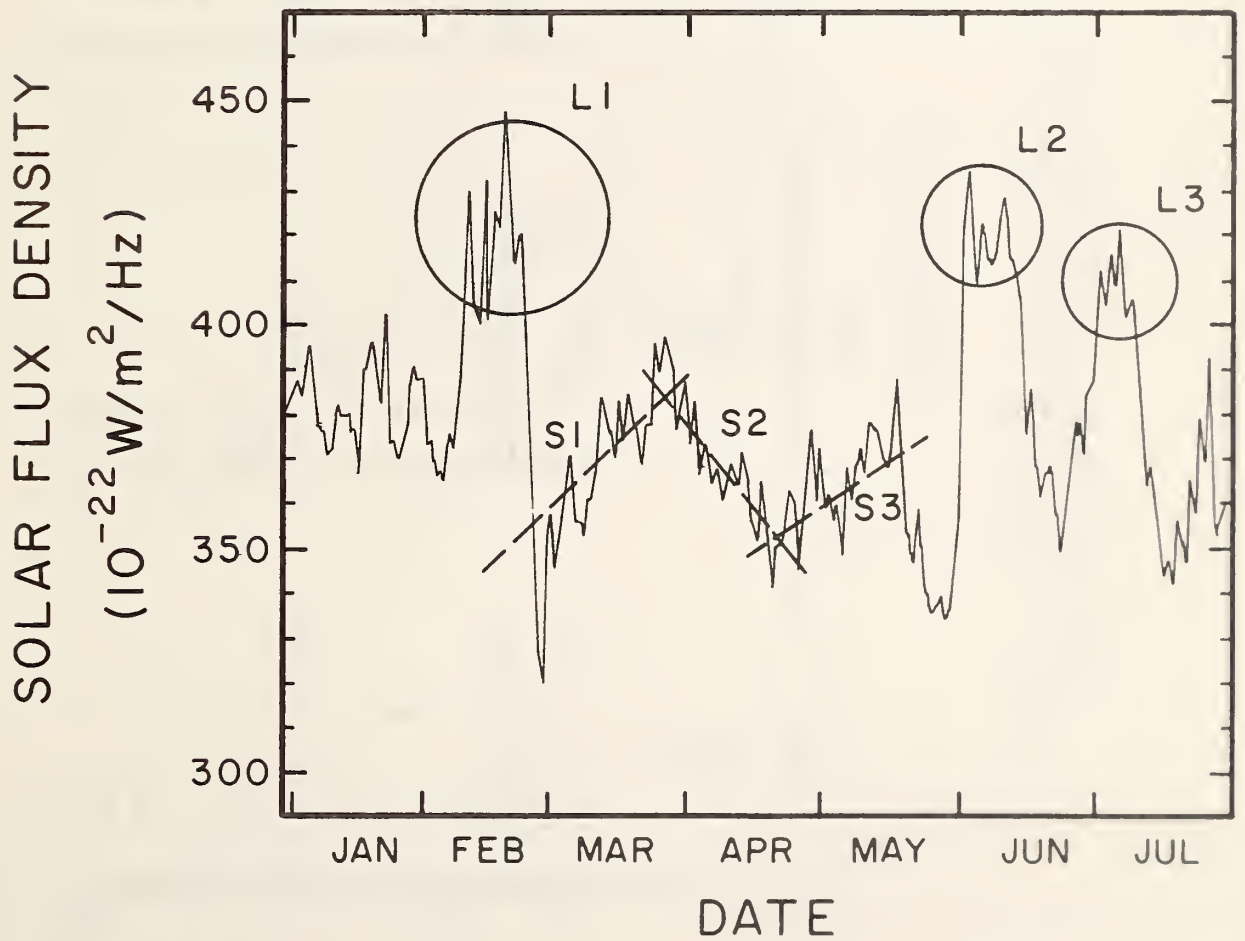
Figure 6. Smoothed solar flux density at 8.8 GHz measured by AFGL from
January to August 1979.
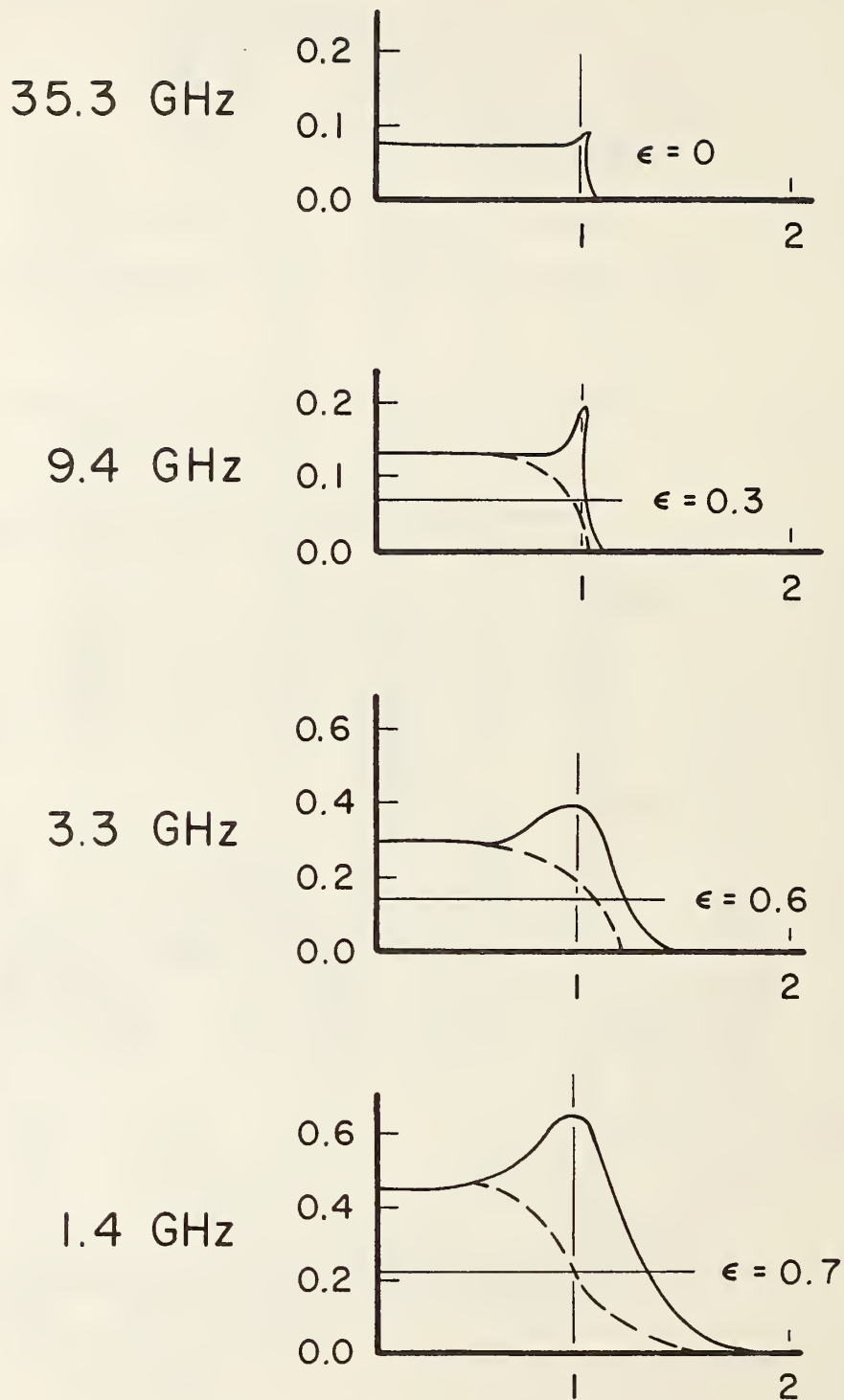
Figure 7. Quiet-sun brightness temperature profiles (in units of 10^5 kelvins) at various frequencies. The solid curves are equatorial profiles, and the dashed curves are polar profiles. The values of ε represent the ellipticity at the half-power levels indicated. The abscissa is in units of the optical solar radius. (After Kundu [9].)
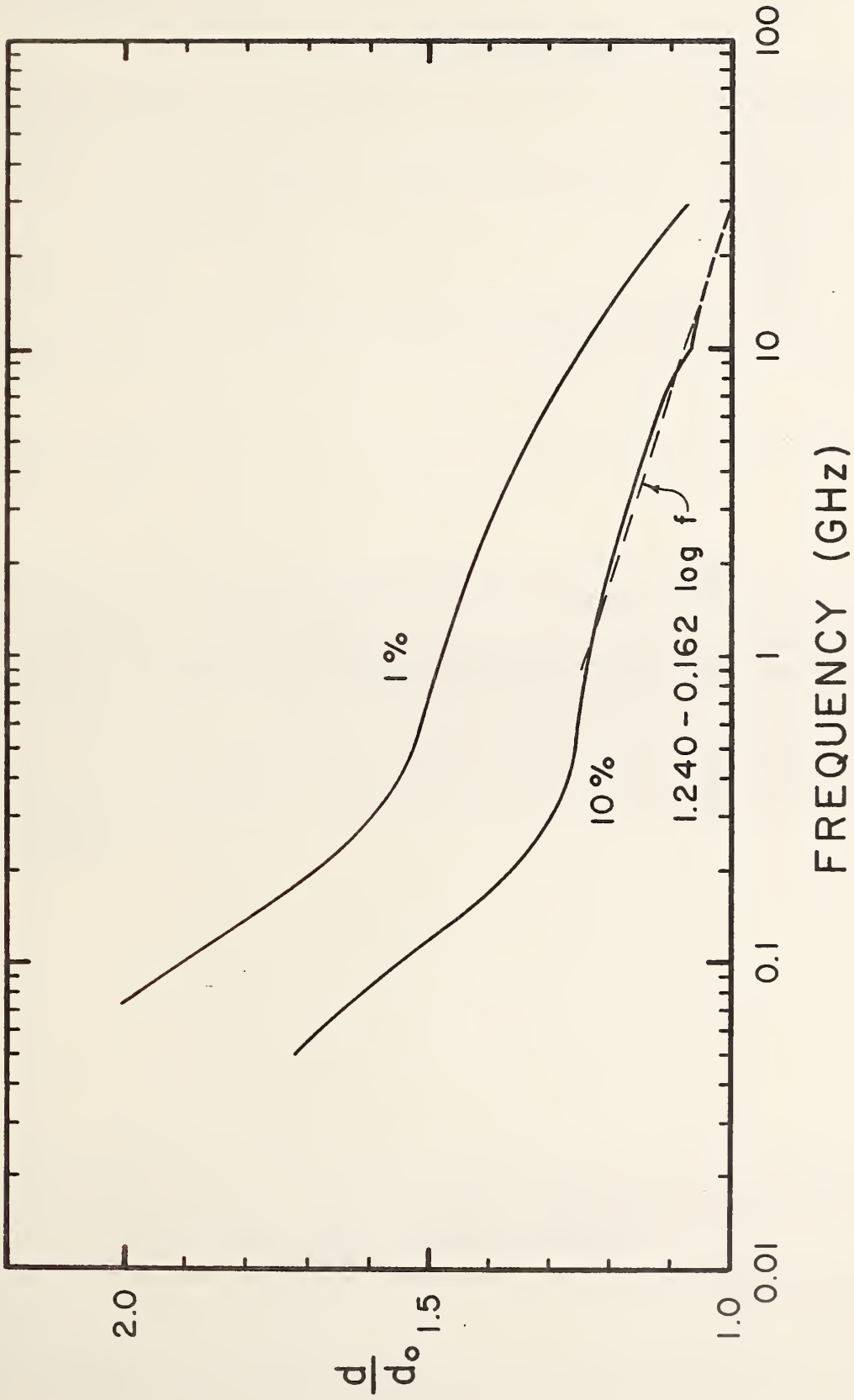
Figure 8. Effective solar rf diameter (d) in units of the optical diameter (d_o) versus frequency for two ratios (1% and 10%) of contour temperature to apparent temperature. (After Smerd [16].)

Table 1. Average flux density $S(W/m^2/Hz)$ versus frequency for the quiet sun radiation in terms of the base-10 logarithm of S. (From Allen [10].)

QUIET SUN RADIATION	
FREQUENCY (GHz)	Log S
10	2.48
20	2.93
50	3.57
100	4.125
200	4.69
500	5.47

U.S. DEPT. OF COMM.	1. PUBLICATION OR REPORT NO.	2. Performing Organ. Report No.	3. Publication Date
BIBLIOGRAPHIC DATA SHEET (See instructions)	NBSIR 84-3015		August 1984

4. TITLE AND SUBTITLE

A Preliminary Investigation Into Using the Sun as a Source for G/T Measurements

5. AUTHOR(S)

William C. Daywitt

6. PERFORMING ORGANIZATION (If joint or other than NBS, see instructions)	7. Contract/Grant No.
NATIONAL BUREAU OF STANDARDS DEPARTMENT OF COMMERCE WASHINGTON, D.C. 20234	8. Type of Report & Period Covered

9. SPONSORING ORGANIZATION NAME AND COMPLETE ADDRESS (Street, City, State, ZIP)

Same as 6

10. SUPPLEMENTARY NOTES

☐ Document describes a computer program; SF-185, FIPS Software Summary, is attached.

11. ABSTRACT (A 200-word or less factual summary of most significant information. If document includes a significant bibliography or literature survey, mention it here)

This report describes a preliminary investigation into determining the solar flux density, the atmospheric correction factor, and the star shape correction factor for use in G/T measurements above 5 GHz. An estimate of errors is also included. Preliminary results show: an improved algorithm for determining diffusive and refractive attenuation; a viable technique for estimating the solar flux density from daily AFGL flux density measurements and a centimeter/millimeter wave spectrum function; and the possibility of reducing star shape correction factor errors by use of·an effective solar rf diameter.

12. KEY WORDS (Six to twelve entries; alphabetical order; capitalize only proper names; and separate key words by semicolons)

atmospheric correction factor; earth terminal measurement system; error analysis; G/T; solar flux density; star shape correction factor

13. AVAILABILITY	14. NO. OF PRINTED PAGES
☒ Unlimited	24
☐ For Official Distribution. Do Not Release to NTIS	
☐ Order From Superintendent of Documents, U.S. Government Printing Office, Washington, D.C. 20402.	15. Price
☒ Order From National Technical Information Service (NTIS), Springfield, VA. 22161	$7.00